Fluorescence of Carotenoids: Probing Binding Site Interactions and Conformational Motion in Carotenoproteins

Justin B. Rose[1] and Warren F. Beck[1,*]

[1]Department of Chemistry, Michigan State University
578 S. Shaw Lane, East Lansing, Michigan 48824 U.S.A.

[*]Corresponding author. Email: beckw@msu.edu

Contents

Abstract

The function of carotenoids in carotenoproteins is optimized by the electrostatic and steric interactions between the carotenoid and its surrounding binding site, which generally imposes distorted conformations and induces charge-transfer character. This chapter shows how the line shape of the fluorescence spectrum, the fluorescence quantum yield, and the fluorescence anisotropy of the second excited singlet state of a carotenoid, S_2, can be used as probes of the structure and dynamics of carotenoids in carotenoproteins. The experimental approach and a brief introduction to the theory we used to detect hydrogen bonding interactions by ketocarotenoids in the orange carotenoid protein are introduced as an example. The fluorescence anisotropy is then introduced as a probe of a carotenoid's excited-state conformational motion using results from a study of β-carotene in solution over a range of temperatures.

1 Introduction

In addition to performing important functions in many organisms by scavenging reactive oxygen species, carotenoids are especially prominent in photosynthetic organisms, where they serve as electronic chromophores capable of capturing mid-visible photons and of quenching

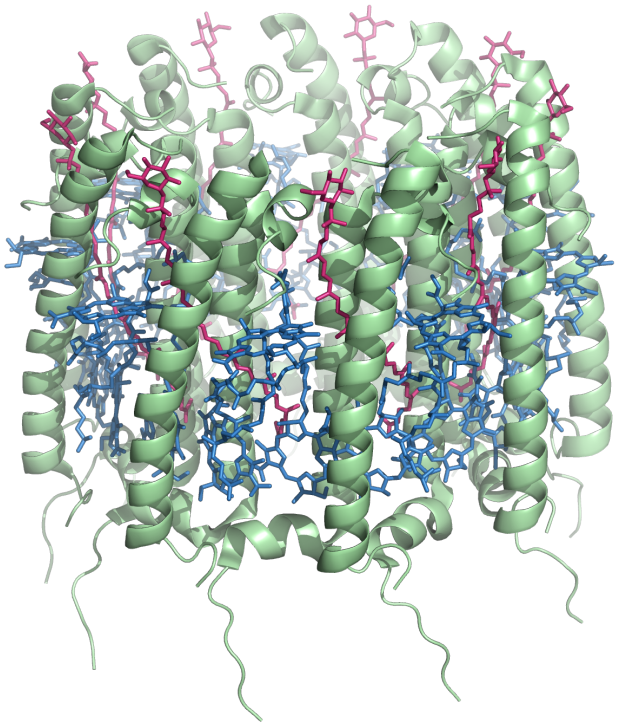

Figure 1: Structure of the LH2 light-harvesting protein from *Rhodopseudomonas acidophila*, as rendered from structure 1NKZ.pdb (Papiz et al., 2003). α helices are shown as green ribbons; the bacteriochlorophyll and rhodopin glucoside chromophores are drawn as cyan and red stick structures, respectively.

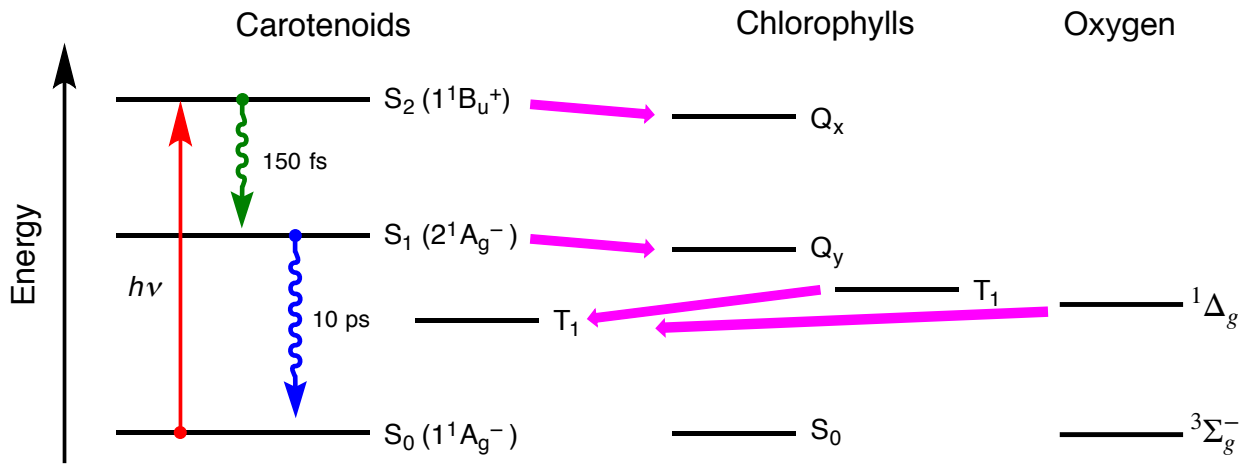

Figure 2: Electronic energy levels for carotenoids, showing singlet and triplet excitation energy transfer between carotenoids and (bacterio)chlorophylls in photosynthetic light-harvesting proteins and quenching of singlet oxygen ($^1\Delta_g$). Nonradiative decay transitions from the S_2 and S_1 states are indicated with wavy arrows. The lifetimes of the states indicated are approximately those of β-carotene. Energy transfer pathways are indicated with filled arrows. After Beck et al. (2015).

triplet excited states in photoprotection mechanisms (Polívka & Frank, 2010). These functions are performed by carotenoids often held in distorted conformations by their binding sites (Beck et al., 2015). For example, consider the helical conformations assumed by the rhodopin glucoside carotenoids in the structure of the LH2 light-harvesting complex in purple bacteria (Fig. 1). In light-harvesting proteins, the carotenoid's singlet excited states S_2 and S_1 (Fig. 2) are found at shorter wavelengths than those of nearby chlorophylls (Chls), allowing them to serve as donor states in excitation energy transfer mechanisms (Polívka & Sundström, 2009). In photoprotection, the energy of a Chl's first excited triplet state, T_1, usually lies above that of a carotenoid, allowing it to serve as a quenching acceptor. But if the Chl triplet survives long enough to transfer its excitation energy to an oxygen molecule, a carotenoid can quench the resulting singlet oxygen species because the energy of its T_1 state usually lies just below that the $^1\Delta_g$ state (Young & Frank, 1996). A given carotenoid bound in a protein site can perform any of these functions because the energies of its singlet and triplet electronic excited states are optimally registered with respect to those of a nearby Chl energy acceptor or triplet donors (Polívka & Sundström, 2004). But the details of how the distorted conformations, the presence of nearby charges, and/or hydrogen-bonding interactions result in tuning of the electronic properties of carotenoids in proteins remains an important question requiring the application of spectroscopic and computational techniques.

Spectroscopic detection of the excited electronic states of carotenoids is usually hampered by their short lifetimes or weak signal strengths. The electric dipole-allowed mid-visible absorption transitions that give rise to the characteristic orange or yellow colors of carotenoid solutions are due to the S_2 state, which exhibits a ~140-fs lifetime in β-carotene, as an example (Ghosh et al., 2015). Despite having a significantly longer lifetime, usually in the 10-ps range, the S_1 state of a carotenoid is usually considered a "dark" state, lacking oscillator

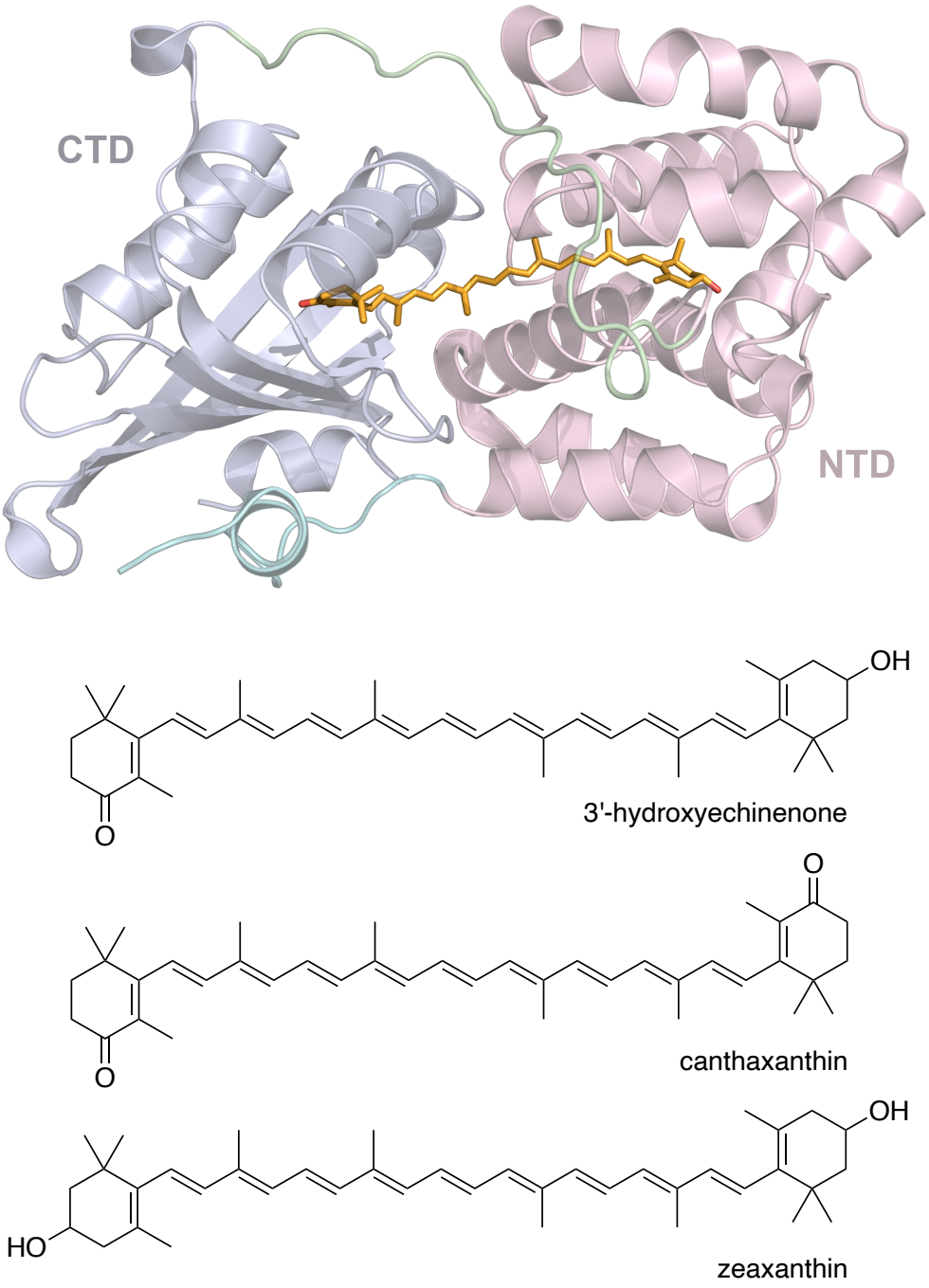

Figure 3: Structures of the orange carotenoid protein (OCP) and of its associated carotenoids. (Top) X-ray crystal structure (5UI2.pdb) in the resting, orange state (OCP^O) of *Arthrospira maxima* (Kerfeld et al., 2003). The N- and C-terminal domains (NTD and CTD, respectively) are rendered as pink and grey ribbons; the peripheral N-terminal α helix and the linker between the NTD and CTD are rendered in green. The bound 3′-hydroxyechinenone (3hECN) is rendered as a stick structure, with carbon atoms in orange and oxygen atoms in red. (Bottom) Structures of three ketocarotenoids that OCP binds: 3hECN, canthaxanthin (CAN), and zeaxanthin (ZEA). After Gurchiek et al. (2018).

strength for electric-dipole allowed transitions to or from the ground state, S_0. In fact, its existence below S_2 was only discovered in the 1980s via its allowed two-photon absorption transitions and then in pump-probe experiments by virtue of strong excited-state absorption transitions to a manifold of higher excited singlet states, S_n (Polívka & Sundström, 2009). Because of the strong absorption transitions to the S_2 state, it is routine to detect carotenoids using resonance Raman spectroscopy, but information on carotenoid conformations is available only in terms of weak signals from non-totally symmetric vibrations (Llansola-Portoles et al., 2017; Mohan T. M. et al., 2021). Although the fluorescence emission from the S_2 state is weak, owing to the short lifetime of the S_2 state, recent studies in our laboratory have shown that considerable information on how a protein binding site controls a carotenoid can be obtained from the fluorescence line shape and emission quantum yield (Gurchiek et al., 2018). These studies provide the basis for the qualitative use of fluorescence information without requiring simulations or a complicated theory, whereas the conformational information available from resonance Raman spectroscopy usually requires an electronic structure calculation followed by a normal-coordinate analysis.

In this chapter, we shall discuss as the main example the experimental methods required to characterize the fluorescence emission from the orange carotenoid protein (OCP), which is employed by cyanobacteria as a light sensor and as a quencher of excitons in the core of the phycobilisome (Fig. 3). The light-sensor function relies on a photoswitching reaction that converts a bound ketocarotenoid, for example 3′-hydroxyechinenone or canthaxanthin, from an orange form, OCP^O, to a red form, OCP^R. The absorption spectrum shifts ~50 nm to the red because the ketocarotenoid adopts a more planar conformation and is exposed to the surrounding aqueous media in the OCP^R state (Leverenz et al., 2015). The ketocarotenoid also is employed in the photoregulatory mechanism when OCP^R binds to the core of the phycobilisome. Hydrogen-bonding interactions between the ketocarotenoid's carbonyl substituent and donors in the in the C-terminal domain (CTD) are thought to be essential in the photoactivation reaction (Kerfeld et al., 2003). The alcohol-substituted carotenoid, zeaxanthin, is accepted in the binding site of OCP but cannot be photoactivated (Punginelli et al., 2009). The example of OCP provides us here a good example of how fluorescence can be used in future work on carotenoproteins because we have observed that the quantum yield of fluorescence of the ketocarotenoids in OCP is enhanced and that the fluorescence line shape is commensurately narrower compared to the same ketocarotenoids in solution (Gurchiek et al., 2018). Further, the likelihood that the ketocarotenoid in OCP undergoes an excited-state change in conformation to initiate the changes in protein structure that follow in the photoactivation mechanism provides an example in which the fluorescence anisotropy can be used as a structural probe. We use results from a recent study of β-carotene in solution (Gurchiek et al., 2020) to show how the anisotropy can be reliably measured in carotenoid systems to determine how a carotenoid's conformation is distorted owing to out-of-plane motions in the S_2 state.

2 Fluorescence Spectrometers for Studies of Carotenoproteins

Although a number of studies have appeared on the fluorescence of carotenoids and related polyenes over the the last thirty years, as reviewed by Gurchiek et al. (2020), our report on the fluorescence of the ketocarotenoids 3hECN and CAN in OCP^O (Gurchiek et al., 2018) is the first for a protein system. The results include the finding that despite the $\sim 10^{-6}$ quantum yield of fluorescence observed for carotenoids in solution, which makes observation of the fluorescence spectrum a technical challenge, the fluorescence from a carotenoid bound in a protein can be several orders of magnitude stronger. The origin of this effect in OCP is that the binding site limits the motions of the carotenoid in the S_2 state with respect to the out-of-plane vibrational coordinates of the isoprenoid backbone that promote nonradiative decay to the S_1 state.

Rather than providing here a comprehensive discussion, the reader is directed to the text by Lakowicz (2011) for coverage of the standard details of fluorescence spectrometers and measurement techniques. We will discuss in the following only the details that we have found necessary for reliable measurements of the fluorescence from carotenoids.

2.1 Excitation Light Source

Fig. 4 shows a schematic diagram for the home-built instrument that we constructed from optical components for our studies of carotenoid fluorescence. The excitation light source is a broadband LED, which is filtered by a compact double monochromator. This combination allows us to obtain a wavelength tunable source of excitation light with ~ 100 cm^{-1} bandpass, which provides enough excitation resolution to allow narrow Raman scattering peaks to be distinguished from the broad fluorescence spectrum. A broadband or "white" LED provides an easily collimatable beam, which is more readily focusable than a standard Xe or tungsten halogen lamp by conventional spherical optics onto the slit of the monochromator. When a compact double monochromator is operated in an additive mode, so that the two gratings result in successive dispersion of the spectrum of light, the stray light background is significantly reduced over that from a single-grating monochromator, especially with the LED light source. In lieu of a broadband light source and a monochromator, a narrow-band laser light source could also be employed. We have performed recent measurements with inexpensive continuous-wave diode lasers, which can be now obtained at single wavelengths across most of the blue and green wavelengths where carotenoids absorb light. Green Nd–YAG or Ar^+ laser sources are routinely used, of course, in measurements of resonance Raman spectra from carotenoid proteins.

2.2 Detection System

After collection and collimation by a lens with a short focal length, the emission from the sample is then focused into the input slit of a single-grating (300 gr/mm) spectrograph with a 0.15 m focal length. Although higher spectral resolutions can be obtained with a longer focal length, the intention here is to record the entire fluorescence spectrum in a single exposure of the CCD detector (~2.5 cm width). This specification rules out use of the long focal-length

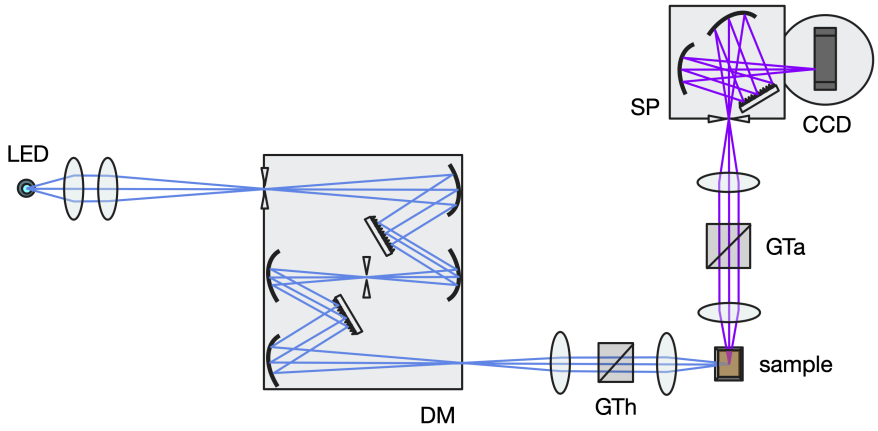

Figure 4: Schematic diagram of the home-built fluorescence spectrometer developed in the authors' laboratory for use in carotenoid fluorescence studies. Symbols: DM, double monochromator; GTh, Glan-Thompson polarizer; GTa, Glan-Taylor polarizer; SP, spectrograph. From Gurchiek et al. (2020), copyright ACS, used with permission.

spectrographs that are commonly used in Raman spectroscopy. The best detector choice is a back-illuminated CCD chip with a low read-out noise level, which allows accumulation of the final spectrum as that accumulated from the sum of several exposures of the CCD. This allows one to employ a statistical filter to remove cosmic-ray spikes from the spectrum. Extended sensitivity into the UV is not required for carotenoids, however, and the usual sensitivity of a Si detector chip out to ~1000 nm will allow detection of the weak emission from the S_1 state of most carotenoids.

To be clear, it is possible but not routine to carry out carotenoid fluorescence spectroscopy with a commercial fluorescence spectrometer equipped with a photomultiplier detector provided that the detection system employs photon counting. But even the red-sensitive photomultipliers in common use are limited to detection of wavelengths below ~800 nm, so detection of emission from the S_1 state would not be possible. With a single-channel photon-counting detection system, measuring a fluorescence spectrum requires scanning the grating of the detection monochromator a step at a time, with sufficient time spent at each wavelength step to count enough photons to obtain an adequate signal/noise ratio. The intensity of the excitation light source will need to be measured simultaneously during the scan by a reference detector so that fluctuations of the light intensity can be removed from the measured spectrum, but this is a standard feature of many commercial instruments. Conventional photomultiplier-based detection systems relying only on measurement of the detected photocurrent are much less sensitive, and it may be difficult to discern the weak carotenoid fluorescence signal from the background unless the detection system includes a lock-in amplifier and the excitation light source is modulated by a mechanical chopper.

2.3 Polarization Optics

As discussed in detail by Lakowicz (2011), measurement of the fluorescence anisotropy requires the use of linear polarizers placed in the excitation and emission beam paths. In our

home-built instrument, a calcite Glan-Thompson polarizer is positioned in the collimated excitation beam prior to the focusing lens. This polarizer is mounted in a standard, manually adjustable rotation stage so that the linear polarization axis of the light can be rotated between the vertical and horizontal planes. A Glan-Taylor polarizer with a much larger aperture is mounted in the collimated emission beam after the collection lens, and here it is preferable to mount the polarizer in a motorized rotation stage so that the polarizer can be rotated under computer control during data acquisition. The procedures we have adopted for use of the polarizers in anisotropy measurements are summarized later in this chapter.

3 Fluorescence Spectra and Raman Interferences

In addition to the challenge of detecting the relatively weak fluorescence spectra from carotenoids in solution and in proteins, it is necessary to distinguish the fluorescence emission from the resonant and non-resonant Raman scattering that will also be present. In solution, because the quantum yield of fluorescence is $\sim 10^{-6}$, resonance Raman signals from the principal vibrations of the carotenoid's isoprenoid backbone, especially the C=C and C–C stretching modes (Llansola-Portoles et al., 2017), will be almost as intense as the fluorescence spectrum. An additional contribution to the spectrum from non-resonant Raman signals from the solution (chiefly water for protein samples) will usually be encountered. Here, although the solvent Raman signals are intrinsically weak owing to their non-resonant character, the solvent molecules are typically present at perhaps 10^5 greater concentration, given that the carotenoid concentration will be about 10 μM in most cases.

Fortunately, we can easily tell the fluorescence emission apart from the Raman signals by taking advantage of the ability to tune the excitation wavelength and to control the spectral band passes of the excitation monochromator and emission spectrograph. The Raman signals are observed at a fixed Stokes shift to lower frequency from the excitation light source corresponding to the vibrational mode frequency, so they move as the excitation wavelength is scanned. Further, the Raman line shapes are much narrower than that of the fluorescence emission for an organic chromophore, and the excitation and emission band passes determine their widths (McHale, 1999; Kelley, 2013).

3.1 Protocol: Recording fluorescence spectra from carotenoproteins

The following protocol provides a routine way to establish which of the features in the spectrum are from fluorescence and which are from Raman scattering. A calibrated emission source is required to correct the recorded emission spectra for the sensitivity with respect to wavelength of the detection system in the fluorescence spectrometer.

3.1.1 Equipment

1. Fluorescence spectrometer and computer system with data acquisition software
2. Excitation polarizer
3. Emission Polarizer

4. calibrated emission source (such as Ocean Optics HL-3P-CAL or LS-1-CAL)
5. fused-silica (quartz) cuvette with 1-cm path length

3.1.2 Chemicals

1. β-Carotene (Sigma-Aldrich C9750)
2. 2-methyltetrahydrofuran (2-MTHF, Sigma-Aldrich 673277)
3. Scattering solution, such as a dilute suspension of non-dairy coffee creamer

3.1.3 Procedure

1. Align the emission polarizer so that it is oriented at the magic angle, 54.7°, with respect to the excitation polarizer. The polarizers are now set to detect a dichroism-free (or unpolarized) fluorescence spectrum (Lakowicz, 2011).
2. Set the slits of the excitation monochromator and emission spectrograph to provide a spectral bandpass of 100 cm^{-1} (~2.5 nm at a wavelength of 500 nm).
3. Record a dark background spectrum; this is an emission spectrum (with the excitation wavelength fixed at a chosen wavelength), but in this case the shutter for the excitation light source should be closed. This spectrum will provide a measure of the signal baseline from the CCD or photon counting system and of any stray light sources. For carotenoids, owing to the usually quite weak emission yield, it may be necessary to cover the sample chamber and detection system of the fluorescence spectrometer with a black cloth or other light isolating material to block ambient light sources in the laboratory. The background spectrum will be subtracted from all of the emission spectra when the data is processed.
4. Prepare a dilute scattering solution using a few crystals of non-dairy coffee creamer in water in the cuvette.
5. Record a calibration emission spectrum, I_{cal}, with the scattering solution in the sample holder of the fluorescence spectrometer illuminated only by the the calibrated emission source. This may require use of a fiber optic or light guide to route light vertically into the sample cuvette.
6. Prepare a solution of β-carotene in the 2-MTHF solution with an absorbance at the 480-nm peak maximum of ~0.2 in a 1-cm fused-silica fluorescence cuvette. Such a solution has a concentration on the order of 10 μM. Because carotenoids absorb very strongly in the mid-visible, it may be required to perform a serial dilution of a more concentrated solution even when dissolving just a few crystals. As discussed by Lakowicz (2011), the usual practice in the measurement of accurate fluorescence emission spectra is to limit the absorption to less than 0.1 in the region of the emission spectrum that overlaps with the absorption spectrum so as to avoid distortion of the emission line shape by self-absorption.

7. Record a series of emission spectra with the β-carotene sample at several fixed excitation wavelengths. Depending on the sensitivity of the detection system and the intensity of the excitation source at the different wavelengths, the number of CCD exposures or scans of the emission monochromator (if a photon-counting system is employed) should be varied to obtain the required signal/noise ratio. When a CCD is used, one should record perhaps 10 equivalent exposures so that spikes in the spectrum due to cosmic rays can be identified.

   Tip: If a CCD camera is used in the detection system, limit the duration of each CCD exposure to avoid having more than a few cosmic ray spikes in a given recording and to keep the sharp features from Raman scattering from being clipped by the maximum CCD signal. The overall signal/noise ratio of the final fluorescence spectrum is principally determined by the total length of time the CCD chip is exposed, so for very weak fluorescence emission from carotenoids in solution, one will require the summation of 10–20 CCD exposures over perhaps 20–45 min total exposure time.

3.1.4 Data Processing

1. If a CCD detector is employed, perform a statistical analysis to identify cosmic ray spikes at different wavelengths in each spectrum. Because cosmic ray spikes involve random incidence of an energetic particle (such as a proton) on the CCD chip, the spikes will not be observed at the same pixel in successive scans. A spike-free spectrum can be calculated by calculating the mean and standard deviation of the number of emission counts at each pixel in the replicate set of exposures. If the count at a particular pixel (emission wavelength) in a given exposure of the CCD exceeds the standard deviation for that pixel, it can be excluded from the linear sum used to calculate the total emission spectrum from the sum of the set of exposures.
2. Subtract the background spectrum from each of the measured emission spectra acquired in the procedure above. Note that the exposure time and the number of replicate scans (or the wavelength step time interval if a photon-counting system is used) needs to be the same for the background spectrum and the measured emission spectra so that the background signal levels and photon-counting statistics are matched.
3. Determine the instrument (wavelength sensitivity) spectrum, I_{inst}, using the I_{cal} spectrum recorded with the calibrated emission source and the absolute intensity spectrum, I_{absol}, provided with it by the manufacturer or by the calibration laboratory: $I_{\text{inst}}(\lambda) = I_{\text{cal}}(\lambda)/I_{\text{absol}}(\lambda)$.
4. For each emission spectrum recorded with the β-carotene sample, $I_{\text{car}}(\lambda)$, calculate the corrected emission spectrum, $F_{\text{car}}(\lambda) = I_{\text{car}}(\lambda) \times I_{\text{inst}}(\lambda)$.

   Tip: It is important to employ a calibrated emission source to determine the instrument sensitivity spectrum especially because even a silicon CCD detector exhibits a rapidly decreasing sensitivity at wavelengths above 800 nm. The emission from the S_1 state, if present, will not be easily detected in the uncorrected spectrum.

3.2 Example: β-Carotene in Hexane

The example of β-carotene in hexane solvent (Fig. 5) shows how the weak fluorescence emission from carotenoids in solution is usually superimposed with sharp Raman scattering line shapes from the carotenoid's isoprenoid backbone and from the solvent and from light scattering at the wavelength of the excitation light. The Raman lines move across the detected spectral range at fixed Stokes shifts (in energy or wavenumber units) from the excitation light scattering peak.

As discussed in (Gurchiek et al., 2018), the spectrum of the fluorescence emission from the S_2 state of a carotenoid is roughly mirror-symmetric with respect to the absorption spectrum. However, the fluorescence spectrum usually exhibits less vibronic structure than the absorption spectrum. The vibronic structure arises from the displacements of the C=C and C–C vibrations of the isoprenoid backbone that occur upon the $\pi \rightarrow \pi^*$ optical excitation, which alters the Franck–Condon factors symmetrically for the absorption and fluorescence vibronic transitions. The depth of the vibronic modulation of the fluorescence spectrum is lessened by a general broadening of the overall fluorescence emission line shape. This phenomenon provides some information on how the excited-state carotenoid interacts more strongly with its surroundings than the ground-state molecule does, chiefly by expansion of the π^* electron density inside the fixed solvent or protein cavity but also due to conformational changes that alter the permanent dipole moment.

Also, note in Fig. 5 that there is a weak emission in the >600-nm region of the fluorescence spectrum that is enhanced when the excitation wavelength is tuned to the bluer wavelengths. This region of the spectrum arises from emission from the S_1 state. The emission from the S_1 state of β-carotene is usually fairly weak (Andersson et al., 1992), but in some carotenoids such as peridinin the S_1 emission is anomalously much stronger than that from S_2 (Greco et al., 2016). As we discussed in a recent study of the S_1 fluorescence from β-carotene (Gurchiek et al., 2020), the relative intensity of the fluorescence emission from the S_2 and S_1 states has to do with the conformation of the isoprenoid backbone of the carotenoid. The S_2 and S_1 states are increasingly mixed as the molecule is twisted, and the intensity of the S_1 state can be considered "borrowed" from the S_2 state.

4 Analysis of Fluorescence Line Shape

Some of the information we want to obtain by measuring the fluorescence spectrum from a carotenoprotein is obtained from the spectral line shape, a plot of the emission oscillator (or dipole) strength as a function of the photon energy or wavenumber (cm^{-1}). The fluorescence line shape carries information on the vibronic structure, the vibrational modes that are stretched upon optical excitation of the carotenoid chromophore. The reader can get the details on this information from a standard molecular spectroscopy textbook, and the ones by McHale (1999) and by Kelley (2013) are recommended. What we want to focus on here, however, is how the breadth of the spectrum tells us how strongly the carotenoid interacts electrostatically with its environment. This information can help us infer how the binding site of a carotenoprotein controls the functional properties of a bound carotenoid.

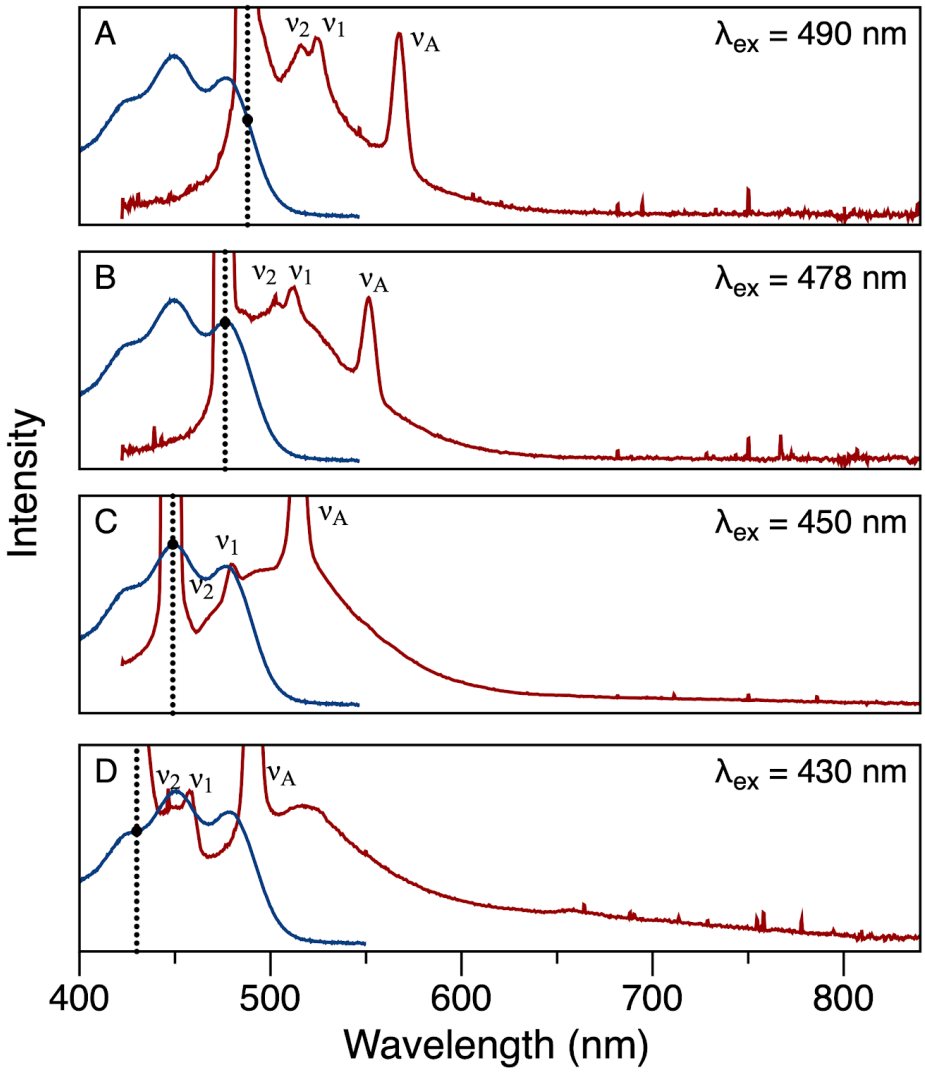

Figure 5: Absorption (blue) and fluorescence emission (red) spectra at four excitation wavelengths from β-carotene in hexane solvent at 23 °C. For the fluorescence spectra, the emission polarizer was oriented at the magic angle (54.6°) with respect to the excitation polarizer. The excitation wavelength is marked in each panel with a vertical dashed line. The positions of resonance Raman peaks from β-carotene (ν_1 = 1517 cm^{-1} and ν_2 = 1157 cm^{-1}) (Saito et al., 1983) and for a non-resonance Raman peak from the hexane solvent (ν_A = 296 cm^{-1}) (Sverdlov et al., 1973) are marked. From Gurchiek et al. (2020), copyright ACS, used with permission.

4.1 Calculation of fluorecence oscillator strength spectra

After measurement of the fluorescence spectrum, the next step is to compare the shape of the fluorescence spectrum with that of the absorption spectrum. by plotting them both as the oscillator (or dipole) strength, the square of the emission transition dipole moment (Cantor & Schimmel, 1980; Lakowicz, 2011), as a function of energy or wavenumber (cm^{-1}) units. The oscillator strength is calculated from the absorption spectrum as $\varepsilon(\nu)/\nu$, where $\varepsilon(\nu)$ gives the molar extinction coefficient with respect to the wavenumber ν. The fluorescence oscillator strength is determined as $\lambda^2 F(\nu)/\nu^3$, where $F(\nu)$ is the number of photon counts as a function of the wavenumber ν (Yu et al., 2002; Ejder, 1969; Melhuish, 1972; Mooney & Kambhampati, 2013). The λ^2 factor compensates for the wavenumber dependence of the throughput of the input aperture determined by the fixed slits of the emission monochromator.

4.2 Example: Ketocarotenoids in the Orange Carotenoid Protein

Fig. 6 compares the absorption and fluorescence spectra from OCP^O preparations at room temperature with either 3hECN or CAN incorporated with that of CAN in chloroform solution. All three of the fluorescence spectra lack mirror symmetry with respect to the absorption spectrum, which indicates that the ketocarotenoid undergoes a structural change upon optical excitation to the S_2 state, but the spectrum from 3hECN in OCP^O is the most symmetric. Just from inspection of the breadth of the fluorescence spectra, one can tell that CAN interacts more strongly than 3hECN overall with its environment. CAN has two carbonyl substitutents, one on each of the β-ionone end rings (Fig. 3), which favor formation of an intramolecular charge-transfer (ICT) character and an increased permanent dipole moment in the S_2 state by withdrawing the π-electron density towards them along the isoprenoid backbone. This induces an increased polarization of the surrounding binding site in the protein. As the strength of the electrostatic interaction between a carotenoid and its surroundings increases, the breadth of the absorption and fluorescence line shapes increases. In the theory of condensed phase spectral line shapes, this interaction strength is measured in terms of the solvation reorganization energy, λ (Fleming & Cho, 1996), which also appears in the Marcus theory for charge transfer; it is not to be confused with the wavelength in this context. The solvation reorganization energy is routinely obtained when mirror symmetry of the absorption and fluorescence spectra is observed by measuring the Stokes shift, 2λ, the difference in wavenumber between the maxima of the oscillator-strength spectra (Kelley, 2013).

5 Detection of Conformational Motion

Although the deviation of the fluorescence line shape from mirror symmetry the absorption spectrum provides an important clue, we can also use the fluorescence quantum yield and anisotropy to infer that a carotenoid is able to move in the binding site of a carotenoid protein. This information is derived from the mechanisms that promote nonradiative decay of the S_2 state to the S_1 state.

The energies of the S_2 and S_1 states converge at a conical intersection as the isoprenoid backbone is distorted with respect to out-of-plane motions of the isoprenoid backbone

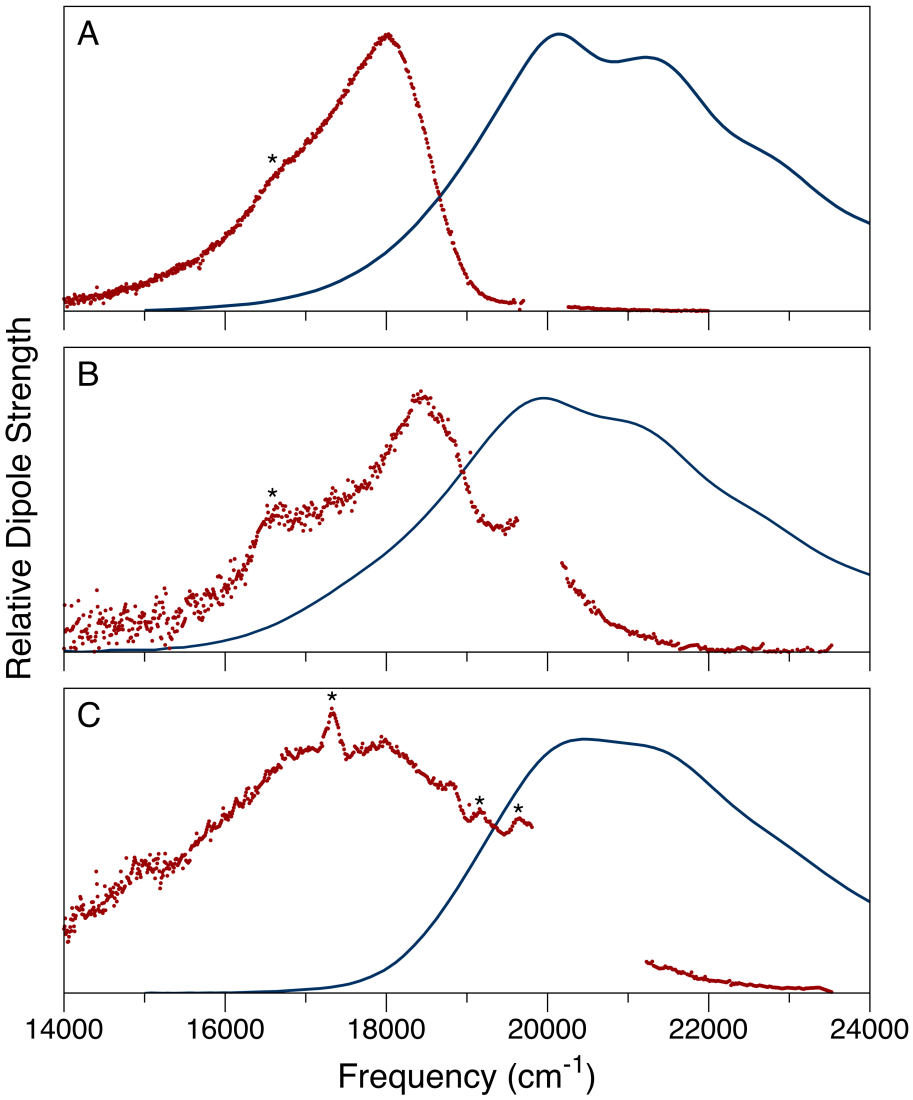

Figure 6: Room-temperature (23 °C) absorption (blue) and fluorescence (red) spectra of carotenoids in OCP^O: (a) 3hECN; (b) CAN; and (c) CAN in chloroform solvent. The intensities are plotted as dipole (or oscillator) strengths, $\varepsilon(\nu)/\nu$ From (Gurchiek et al., 2018), copyright ACS, and $\lambda^2 F(\nu)/\nu^3$, respectively, with normalization to peak intensity. The excitation monochromator for the fluorescence was tuned to 500 nm (20000 cm^{-1}) for panels (a) and (b) and to 490 nm (20408 cm^{-1}) for (c). In panels (a) and (b), the asterisk at 16500 cm^{-1} marks the wavenumber of the nonresonant Raman band from water (shift of 3500 cm^{-1}). In panel (c), asterisks nonresonant Raman bands from the chloroform solvent at 17340, 19160, and 19640 cm^{-1} (shifts of 3034, 1220, and 774 cm^{-1}) (Shimanouchi, 1972). From Gurchiek et al. (2018), copyright ACS, used with permission.

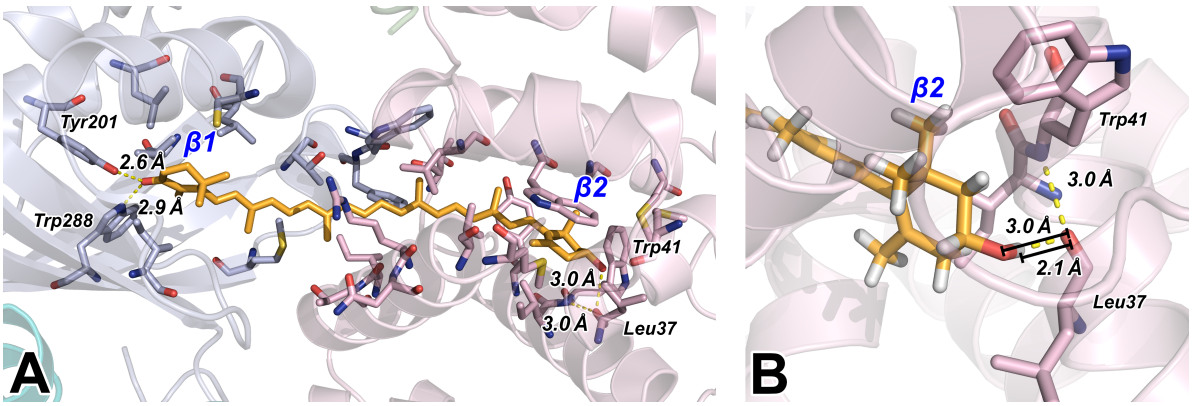

Figure 7: Protein–ketocarotenoid hydrogen bonding interactions between 3hECN and groups in the binding site of OCP^O from *Synechocystis* sp. PCC 6803, as rendered using structure 5TV0.pdb (Bandara et al., 2017). (a) View of the overall binding site, showing the interactions of the β-ionone rings $\beta 1$ and $\beta 2$ in the CTD and NTD, respectively. (b) Detail from a rotated vantage point of the $\beta 2$ ring's hydrogen bonding interaction between the hydroxyl group and the carbonyl on Leu37. From Gurchiek et al. (2018), copyright ACS, used with permission.

(Gurchiek et al., 2020). As a result, after a carotenoid absorbs a photon, it undergoes ultrafast structural distortions during the lifetime of the S_2 state that tend to twist and bend the isoprenoid backbone. This motion can be detected in two complementary ways:

1. **Fluorescence Quantum Yield.** Because the out-of-plane motions quench the fluorescence from the S_2 state by promoting nonradiative decay to the S_1 state, the lifetime of the S_2 state depends on the ability of the carotenoid to move inside the binding site. For example, the S_2 state lifetime of β-carotene is 140 fs (Ghosh et al., 2015), whereas the lifetime of the S_2 state of CAN in toluene solution is significantly longer because of the friction resulting from its carbonyl-induced ICT character (Mohan T. M. et al., 2021). In other words, if the S_2 can move easily in the binding site in a carotenoid protein, the fluorescence quantum yield, the fraction of absorbed photons that result in emission of a fluorescence photon will be correspondingly low (Gurchiek et al., 2018).

2. **Fluorescence Anisotropy.** As the isoprenoid backbone of the carotenoid twists at one or more of the C=C bonds, the direction of the emission transition dipole moment (TDM) of the S_2 state is rotated with respect to its initial direction, that of the molecule in the ground state prior to absorption of a photon. Accordingly, fluorescence anisotropy measurements can be used to sense the direction of the TDM in the S_2 and sometimes in the S_1 state. The direction of the TDM for carotenoids is closely aligned with respect to the direction of the isoprenoid backbone; electronic structure calculations show that torsional or pyramidal distortions at C=C bonds causes a rotation of the TDM that reflects the vectorial sum of the directions of the isoprenoid chains on either end of the molecule (Gurchiek et al., 2020).

5.1 Protocol: Measurement of fluorescence quantum yield

Although the fluorescence quantum yield can be measured in absolute terms using more elaborate apparatus, it is more common to determine the *relative* quantum yield using a well-characterized fluorescent dye, such as Rhodamine 6G, as an emission yield standard. As outlined below, the procedure is to measure the integrated fluorescence oscillator strength for the carotenoprotein and the standard dye with the same fluorescence spectrometer. The total fluorescence emission from the two solutions is compared after compensating them for the different strengths of absorption and intensities of the excitation light.

5.1.1 Chemicals

1. Rhodamine 6G (Sigma-Aldrich, C9750)
2. methanol (Sigma-Aldrich, 673277)

5.1.2 Procedure

1. As preliminary steps, follow the protocol in section 3.1 to set up the fluorescence spectrometer and to prepare a solution of the carotenoid or carotenoprotein.
2. Prepare a solution of rhodamine 6G (or another suitable fluorescent dye), also with a maximum absorbance of ~0.2 in a 1-cm fused-silica fluorescence cuvette.
3. Record absorption spectra of the carotenoid and rhodamine 6G solutions.
4. Also following section 3.1, record fluorescence emission spectra of the carotenoid and rhodamine 6G solutions, noting the excitation wavelengths and the integration times used in both measurements.

   Tip: If the absorption spectra of the carotenoid and rhodamine 6G solutions have overlapping wavelength ranges, use the same excitation wavelength for measurement of their fluorescence spectra. If this is not possible, measure the intensity of the incident excitation light beam using a silicon photodiode or a power meter at both wavelengths.

5.1.3 Data Processing

1. Following the procedures in section 3.1.4 and section 4.1, determine the oscillator strength spectra for the carotenoid and rhodamine 6G standard.
2. Normalize the fluorescence oscillator strength spectra of the carotenoid and of the rhodamine 6G standard by dividing them by the total integration time used to acquire their spectra. The quantum yield of rhodamine 6G is 0.93 in methanol (Magde et al., 2002), so the integration time required to obtain a high quality spectrum will be much shorter than that required for the carotenoid. For example, assuming the quantum yield of fluorescence of the carotenoid is 10^{-6} and a 20-min exposure time is required to record its fluorescence spectrum, the total CCD exposure time to obtain the same signal/noise ratio for the rhodamine 6G solution would be only 1.3 ms. In practice, of

course, the signal/noise ratio of the rhodamine 6G spectrum is much higher than that of the carotenoid even with the shortest practical CCD exposure times.

3. If the excitation wavelengths used for the fluorescence measurements of the carotenoid and the rhodamine 6G standard were not the same, then normalize each of the fluorescence oscillator strength spectra by dividing them by the intensity of the excitation light.

4. Using a data graphing program, determine the integrals F_{int} of the fluorescence oscillator strength spectra from the carotenoid and the rhodamine 6G standard after normalization of the spectra.

   Tip: In order to exclude the interfering Raman features and scattered excitation light from the integral of the carotenoid spectrum, a good approach here is to fit it to a log-normal (asymmetric Gaussian) line shape (Siano & Metzler, 1969). Because the log-normal function is normalized (unit area), the scaling factor for the fitted line shape provides the total area under the line shape due to fluorescence.

5. Using the sample absorbances A and indices of refraction, n, at the excitation wavelengths used for the fluorescence measurements for the carotenoid (car) and Rhodamine 6G (std) solutions, compute the quantum yield of fluorescence Φ_f for the carotenoid using the following equation (Andersson et al., 1992):

$$\Phi_{f,\text{car}} = \Phi_{f,\text{std}} \frac{F_{\text{int,car}}}{F_{\text{int,std}}} \frac{[1 - 10^{-A_{\text{std}}} n_{\text{car}}^2]}{[1 - 10^{-A_{\text{car}}} n_{\text{std}}^2]} \tag{1}$$

5.2 Example: Ketocarotenoids in the Orange Carotenoid Protein

As determined using the protocol above and the fluorescence spectra shown in Fig. 6, the absolute fluorescence quantum yields for 3hECN and CAN in OCP^O are 3.8×10^{-3} and 6.0×10^{-4}, respectively. In contrast, the fluorescence quantum yield for CAN in chloroform solvent is 4.0×10^{-6} (Gurchiek et al., 2018). These quantum yields are consistent with the relative signal/noise ratio of the three spectra.

The enhanced fluorescence quantum yield for 3hECN compared to that for CAN in OCP^O indicates that there is an additional interaction in its ketocarotenoid binding site that restricts its motion in the S_2 state. Given knowledge of this effect, we compared the X-ray crystal structures of OCP^O determined by X-ray diffraction with 3hECN and CAN bound. This analysis revealed that 3hECN makes a previously undetected hydrogen-bonding interaction between the 3′-hydroxyl group on its $\beta 2$ ring and the peptide backbone at Leu37 in the NTD of OCP (Fig. 7) An analogous hydrogen bond cannot be formed by CAN because the carbonyl substituent on its $\beta 2$ cannot serve as a hydrogen-bond donor (Gurchiek et al., 2018).

5.3 Protocol: Measurement of Fluorescence Anisotropy

The fluorescence anisotropy, r, is usually obtained from separate measurements of the linearly polarized components of the fluorescence emission at two orientations, parallel (||) and

perpendicular ($\perp$), with respect to the plane of linear polarization of the excitation light source (Lakowicz, 2011).

$$r = \frac{F_{\parallel} - F_{\perp}}{F_{\parallel} + 2F_{\perp}} \tag{2}$$

In order to perform these measurements, the detection system of the fluorescence spectrometer requires a calcite polarizer that can be rotated manually or under computer control.

When measuring the fluorescence anisotropy of solutions of carotenoproteins, the signal/noise ratio and the fidelity of the anisotropy spectrum is improved by measuring the magic-angle fluorescence spectrum, F_M, instead of measuring $F_{\parallel}$. Because the interfering Raman scattering line shapes are highly polarized, shorter CCD exposures are required to avoid saturation or clipping if $F_{\parallel}$ is detected. The protocol that follows shows how to calculate the anisotropy using F_M and $F_{\perp}$ and to calibrate the detection system to compensate for its sensitivity to the different orientations of the emission polarizations. The reader should consult the comprehensive text by Lakowicz (2011) for additional details.

5.3.1 Chemicals

1. Rhodamine 6G (Sigma-Aldrich 252433)
2. LD 425 (Exciton 04250)
3. LDS 765 (Exciton 07650)
4. methanol (Sigma-Aldrich 322415)

5.3.2 Procedure

1. As a preliminary step, set up the fluorescence spectrometer and prepare a solution of the carotenoid or carotenoprotein, as indicated in section 3.1.
2. Prepare solutions of rhodamine 6G, LD 425, and LDS 765 in methanol to obtain a maximum absorbance of ~0.2 in a 1-cm fused-silica fluorescence cuvette. The fluorescence spectra of the three dyes specified here overlap over the 450–1000 nm range of emission wavelengths.
3. With the excitation polarizer in the fluorescence spectrometer rotated to the horizontal (H) orientation, record fluorescence spectra for the three dye solutions with the emission polarizer rotated to the horizontal (H) and vertical (V) orientations. Consult the procedure listed in section 3.1 for the required steps.
4. Also with the three dyes, measure three additional fluorescence spectra, F_{VV}, F_{VM}, and F_{VH}, where the subscripts indicate the (excitation, emission) polarizer orientations.
5. Now record the F_{VM} and F_{VH} fluorescence emission spectra of the carotenoprotein solution.

5.3.3 Data Processing

1. Using the spectra measured for the three dyes, calculate the ratio

$$G = \frac{F_{HV}}{F_{HH}} \tag{3}$$

where the subscripts indicate the (excitation, emission) polarizer directions.

2. Also with the spectra for the three dyes, calculate the VM correction (Gurchiek et al., 2020),

$$C = \frac{2GF_{VH} + F_{VV}}{F_{VM}} \tag{4}$$

Tip: The G and C spectra are used to correct the relative sensitivities of the detection system in the fluorescence spectrometer for emission with different polarization orientations. In particular, the choice of the blaze wavelength for the diffraction grating in the emission spectrograph causes certain wavelength regions to be detected more sensitively. To cover the entire range of a carotenoid's fluorescence spectrum, plot the G or C spectra measured for the three dyes on the same set of axes and then construct a smooth polynomial function that fits the overlapping spectra.

3. Now using the spectra measured for the carotenoprotein, calculate the fluorescence anisotropy,

$$r = \frac{CF_{VM} - 3GF_{VH}}{CF_{VM}} \tag{5}$$

Tip: Because the anisotropy r is calculated as a ratio of two spectra, it is not necessary to perform the data processing steps above with oscillator-strength spectra. The computed r spectrum can be plotted equivalently with respect to wavelength or wavenumber without distortion.

5.4 Example: β-Carotene in 2-MTHF solution

Although we have not yet published a study of the fluorescence anisotropy with OCP preparations, we have carried out a comprehensive study of fluorescence anisotropy in β-carotene solutions over a range of cryogenic temperatures (Gurchiek et al., 2020) that provides a useful example of the information that we anticipate can be gained in proteins.

Fig. 8 shows the temperature dependence of the absorption, fluorescence emission, and fluorescence anisotropy spectra over the 80–258 K temperture range. At low temperatures, the isoprenoid backbone of β-carotene is hindered by the glassy 2-MTHF solvent surrounding it, so the anisotropy r is high, ~ 0.36, and constant with respect to the emission wavenumber. The maximum value possible for r is 0.4, which is observed when the absorption and emission TDMs are exactly parallel (Lakowicz, 2011). As the temperature is raised, however, the viscosity of the solvent decreases markedly, and r decreases, showing that the isoprenoid backbone has undergone a twisting and/or pyramidal deformation near its center. At 258 K, $r \approx 0.2$, which corresponds closely to the anisotropy calculted for the pyramidal structure

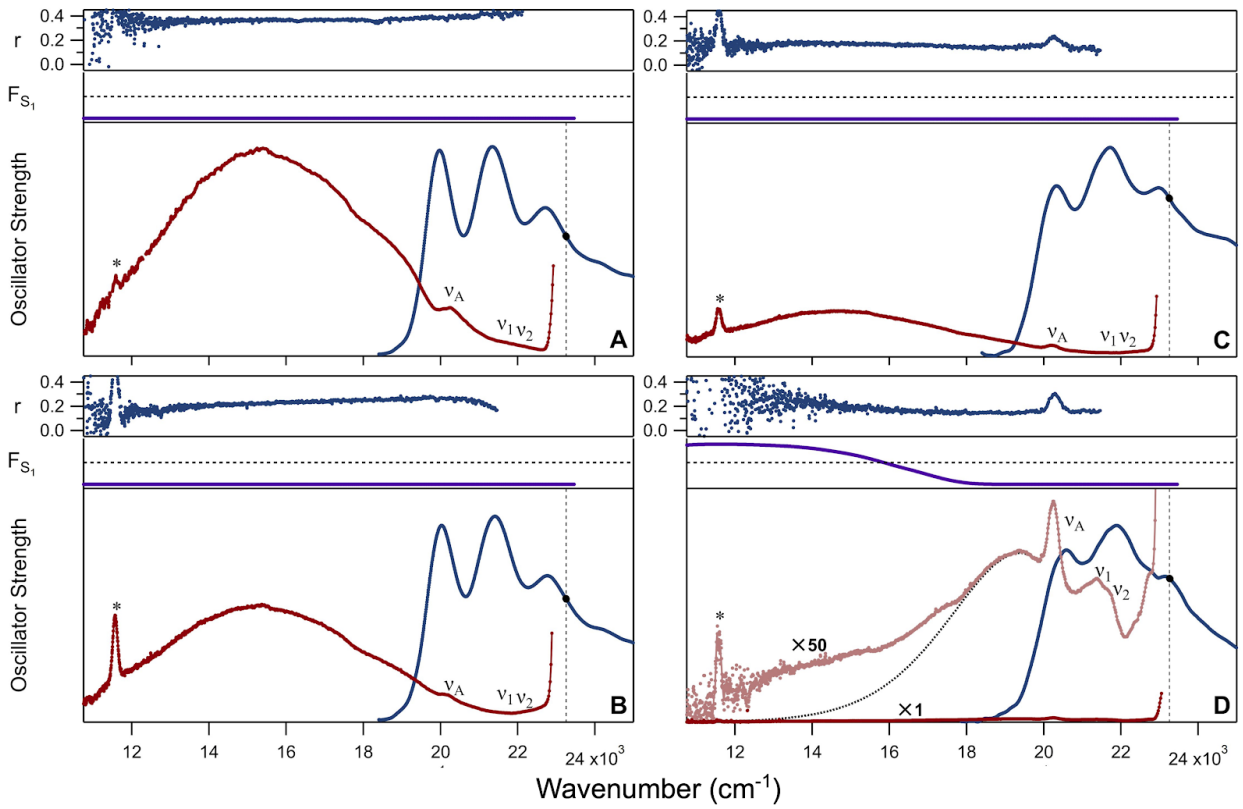

Figure 8: Fluorescence oscillator strength and anisotropy (r) spectra for β-carotene in 2-MTHF solvent at 293 K with excitation at 430 nm (23,250 cm^{-1}) at four temperatures: (a) 80 K; (b) 120 K; (c) 200 K; and (d) 258 K. The excitation wavenumber is marked in each panel with a vertical dashed line. The absorption oscillator strength (blue) is arbitrarily scaled to mirror that of the S_2 fluorescence emission line shape. A baseline for the S_1 emission is suggested by a log-normal line shape for the red tail of the S_2 emission. F_{S_1} (purple) estimates the fraction of the fluorescence oscillator strength from the S_1 state; $F_{S_1} = 0.5$ is marked by the dashed line. The positions of resonance Raman peaks from β-carotene (ν_1 = 1517 cm^{-1} and ν_2 = 1157 cm^{-1}) (Saito et al., 1983) and for a non-resonance Raman peak from the 2-MTHF solvent (ν_A = 2915 cm^{-1}) (Durig et al., 1973) are marked. From Gurchiek et al. (2020), copyright ACS, used with permission.

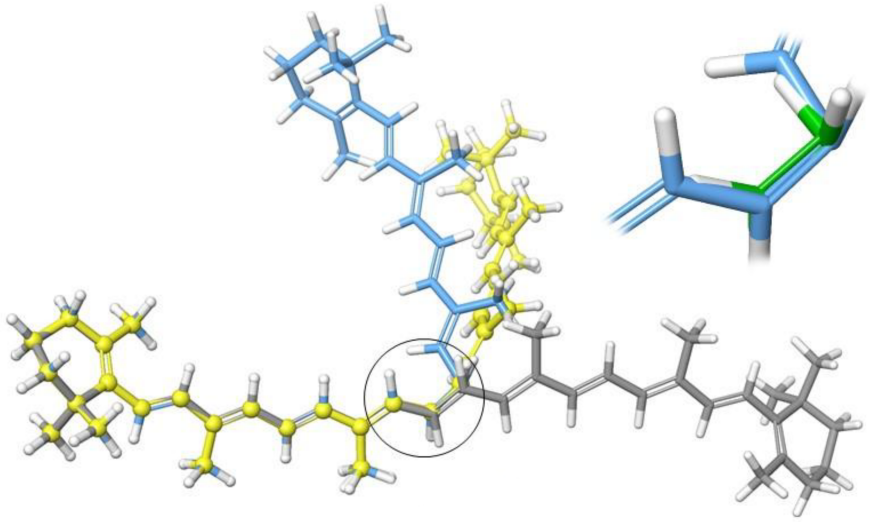

Figure 9: Modeled structures representing for β-carotene the Franck-Condon S_2 structure (gray), the 90° twisted conformer (yellow), and a conformer with a pyramidal distortion (light blue). The inset is a zoomed-in view of the circled region, which shows the modeled pyramidal structure superimposed with the pyramidal conical intersection structure of ethylene (green) (Minezawa & Gordon, 2009). From Gurchiek et al. (2020), copyright ACS, used with permission.

shown in Fig. 9 (Gurchiek et al., 2020). As the fluorescence anisotropy decreases, the intensity of a broad emission from a twisted intermediate of the S_2 state decreases. This result shows a comparison of the fluorescence emission and anisotropy spectra may allow one to distinguish between distortions of a single C=C bond in a carotenoid from distortions of more than one C=C bond, such as in the bicycle-pedal structure suggested for retinal by Warshel (1976).

6 Summary

Although measurement of the fluorescence properties of a carotenoid in a carotenoprotein is considerably more challenging than performing similar measurements on conventional fluorescence probes with higher quantum yields, our experience with the methods described in this chapter indicates that reliable information can be obtained that provides some unprecedented information on the interactions between a carotenoid and its binding site in a carotenoprotein that is not available presently from other measurements. The use of fluorescence line shape, quantum yield, and anisotropy information comes from the point-of-view that the emission from a carotenoid is *dynamic* in character (Gurchiek et al., 2020); because the emission from the S_2 state is short lived and occurs while the carotenoid is moving towards a conical intersection with the S_1, where nonradiative decay occurs, there is considerably more information available than is usually encountered with conventional fluorescent probes. We hope that the example discussed in this chapter of how we obtained new information on the structure and function of the OCP will inspire similar investigations of other carotenoproteins in the future. Further, we should point out that the methods introduced here could also be applied to studies of photoswitching reactions of protonated

Schiff bases, as in the rhodopsins, or of the bilin chromophores in phytochrome or other cyanobacteriochromes.

Acknowledgment

Work in the laboratory of W.F.B. was principally supported by grant award DE-SC0010847 from the Photosynthetic Systems program of the Office of Basic Energy Sciences, U.S. Department of Energy. Additional support for in-common instrumentation was from grant award DE-SC0021197 from the Solar Photochemistry program of the Office of Basic Energy Sciences, U.S. Department of Energy, and from grant award 1904655 from the Chemistry of Life Processes program of the U.S. National Science Foundation. We acknowledge collaboration on the OCP studies with the laboratory of Professor Cheryl A. Kerfeld, which is supported by grant award DE-SC0020606 from the Photosynthetic Systems program of the Office of Basic Energy Sciences, U.S. Department of Energy.

References

Andersson, P. O., Gillbro, T., Asato, A. E., & Liu, R. S. H. (1992). Dual singlet state emission in a series of mini-carotenes. *J. Lumin.*, *51*, 11–20. doi: 10.1016/0022-2313(92)90014-Z

Bandara, S., Ren, Z., Lu, L., Zeng, X., Shin, H., Zhao, K. H., & Yang, X. (2017). Photoactivation mechanism of a carotenoid-based photoreceptor. *Proc. Natl. Acad. Sci. U. S. A.*, *114*, 6286–6291. doi: 10.1073/pnas.1700956114

Beck, W. F., Bishop, M. M., Roscioli, J. D., Ghosh, S., & Frank, H. A. (2015). Excited state conformational dynamics in carotenoids: dark intermediates and excitation energy transfer. *Arch. Biochem. Biophys.*, *572*, 175–183. doi: 10.1016/j.abb.2015.02.016

Cantor, C. R., & Schimmel, P. R. (1980). *Biophysical Chemistry. Part II: Techniques for the Study of Biological Structure and Function*. San Francisco: W. H. Freeman and Company.

Durig, J. R., Kizer, K. L., & Karriker, J. M. (1973). Spectra and structure of small ring compounds. XXXVI. 2-methyl-1,3-dioxolane; 2-methyl-1,3-dioxolane-d_4; 2-methyltetrahydrofuran; and methylcyclopentane. *J. Raman Spectrosc.*, *1*, 17–45. doi: 10.1002/jrs.1250010103

Ejder, E. (1969). Methods of representing emission, excitation, and photoconductivity spectra. *J. Opt. Soc. Amer.*, *59*, 223–224.

Fleming, G. R., & Cho, M. (1996). Chromophore-solvent dynamics. *Annu. Rev. Phys. Chem.*, *47*, 109–134. doi: 10.1146/annurev.physchem.47.1.109

Ghosh, S., Bishop, M. M., Roscioli, J. D., Mueller, J. J., Shepherd, N. C., LaFountain, A. M., ... Beck, W. F. (2015). Femtosecond heterodyne Transient-Grating studies of nonradiative decay of the S_2 ($1^1B_u^+$) state of β-Carotene: Contributions from dark intermediates and Double-Quantum coherences. *J. Phys. Chem. B*, *119*, 14905–14924. doi: 10.1021/acs.jpcb.5b09405

Greco, J. A., LaFountain, A. M., Kinashi, N., Shinada, T., Sakaguchi, K., Katsumura, S., ... Frank, H. A. (2016). Spectroscopic investigation of the carotenoid deoxyperidinin: direct observation of the forbidden $S_0 \rightarrow S_1$ transition. *J. Phys. Chem. B*, *120*, 2731–2744. doi: 10.1021/acs.jpcb.6b00439

Gurchiek, J. K., Bao, H., Domínguez-Martín, M. A., McGovern, S. E., Marquardt, C. E., Roscioli, J. D., ... Beck, W. F. (2018). Fluorescence and excited-state conformational dynamics of the orange carotenoid protein. *J. Phys. Chem. B*, *122*, 1792–1800. doi: 10.1021/acs.jpcb.7b09435

Gurchiek, J. K., Rose, J. B., Guberman-Pfeffer, M. J., Tilluck, R. W., Ghosh, S., Gascón, J. A., & Beck, W. F. (2020). Fluorescence anisotropy detection of barrier crossing and ultrafast conformational dynamics in the S_2 state of β-carotene. *J. Phys. Chem. B*, *124*, 9029–9046. doi: 10.1021/acs.jpcb.0c06961

Kelley, A. M. (2013). *Condensed-Phase Molecular Spectroscopy and Photophysics*. Hoboken, New Jersey: John Wiley & Sons.

Kerfeld, C. A., Sawaya, M. R., Brahmandam, V., Cascio, D., Ho, K. K., Trevithick-Sutton, C. C., ... Yeates, T. O. (2003). The crystal structure of a cyanobacterial water-soluble carotenoid binding protein. *Structure*, *11*, 55–65. doi: 10.1016/S0969-2126(02)00936-X

Lakowicz, J. R. (2011). *Principles of Fluorescence Spectroscopy* (3rd ed.). New York: Springer US. doi: 10.1007/978-0-387-46312-4

Leverenz, R. L., Sutter, M., Wilson, A., Gupta, S., Thurotte, A., de Carbon, C. B., … Kerfeld, C. A. (2015). A 12 Å carotenoid translocation in a photoswitch associated with cyanobacterial photoprotection. *Science*, *348*, 1463–1466. doi: 10.1126/science.aaa7234

Llansola-Portoles, M. J., Pascal, A. A., & Robert, B. (2017). Electronic and vibrational properties of carotenoids: from *in vitro* to *in vivo*. *J. R. Soc. Interface*, *14*, 20170504. doi: 10.1098/rsif.2017.0504

Magde, D., Wong, R., & Seybold, P. G. (2002). Fluorescence quantum yields and their relation to lifetimes of rhodamine 6G and fluorescein in nine solvents: improved absolute standards for quantum yields. *Photochem. Photobiol.*, *75*, 327–334. doi: 10.1562/0031-8655(2002)0750327FQYATR2.0.CO2

McHale, J. L. (1999). *Molecular Spectroscopy*. Upper Saddle River, New Jersey: Prentice Hall.

Melhuish, W. H. (1972). Absolute spectrofluorimetry. *J. Res. Natl. Bur. Stand.*, *76A*, 547–560. doi: 10.6028/jres.076A.049

Minezawa, N., & Gordon, M. S. (2009). Optimizing conical intersections by spin-flip density functional theory: application to ethylene. *J. Phys. Chem. A*, *113*, 12749–12753. doi: 10.1021/jp908032x

Mohan T. M., N., Leslie, C. H., Sil, S., Rose, J. B., Tilluck, R. W., & Beck, W. F. (2021). Broadband 2DES detection of vibrational coherence in the S_x state of canthaxanthin. *J. Chem. Phys.*, *155*, 035103. doi: 10.1063/5.0055598

Mooney, J., & Kambhampati, P. (2013). Get the basics right: Jacobian conversion of wavelength and energy scales for quantitative analysis of emission spectra. *J. Phys. Chem. Lett.*, *4*, 3316–3318. doi: 10.1021/jz401508t

Papiz, M. Z., Prince, S. M., Howard, T., Cogdell, R. J., & Isaacs, N. W. (2003). The structure and thermal motion of the B800-850 LH2 complex from *Rps. acidophila* at 2.0 Å resolution and 100 K: New structural features and functionally relevant motions. *J. Mol. Biol.*, *326*, 1523–1538. doi: 10.1016/S0022-2836(03)00024-X

Polívka, T., & Frank, H. A. (2010). Molecular factors controlling photosynthetic light harvesting by carotenoids. *Acc. Chem. Res.*, *43*, 1125–1134. doi: 10.1021/ar100030m

Polívka, T., & Sundström, V. (2004). Ultrafast dynamics of carotenoid excited states—from solution to natural and artificial systems. *Chem. Rev.*, *104*, 2021–2071. doi: 10.1021/cr020674n

Polívka, T., & Sundström, V. (2009). Dark excited states of carotenoids: consensus and controversy. *Chem. Phys. Lett.*, *477*, 1–11. doi: 10.1016/j.cplett.2009.06.011

Punginelli, C., Wilson, A., Routaboul, J. M., & Kirilovsky, D. (2009). Influence of zeaxanthin and echinenone binding on the activity of the orange carotenoid protein. *Biochim. Biophys. Acta*, *1787*, 280–288. doi: 10.1016/j.bbabio.2009.01.011

Saito, S., Tasumi, M., & Eugster, C. H. (1983). Resonance Raman spectra (5800–40 cm^{-1}) of all-*trans* and 15-*cis* isomers of β-carotene in the solid state and in solution. measurements with various laser lines from ultraviolet to red. *J. Raman Spectrosc.*, *14*, 299–309. doi: 10.1002/jrs.1250140503

Shimanouchi, T. (1972). *Tables of Molecular Vibrational Frequencies Consolidated Volume I*. National Bureau of Standards.

Siano, D. B., & Metzler, D. E. (1969). Band shapes of the electronic spectra of complex molecules. *J. Chem. Phys.*, *51*, 1856–1861. doi: 10.1063/1.1672270

Sverdlov, L. M., Kovner, M. A., & Kraĭ. (1973). *Vibrational Spectra of Polyatomic Molecules*. John Wiley & Sons.

Warshel, A. (1976). Bicycle-pedal model for the first step in the vision process. *Nature*, *260*, 679–683. doi: 10.1038/260679a0

Young, A. J., & Frank, H. A. (1996). Energy transfer reactions involving carotenoids: quenching of chlorophyll fluorescence. *J. Photochem. Photobiol. B*, *36*, 3–15. doi: 10.1016/S1011-1344(96)07397-6

Yu, A., Tolbert, C. A., Farrow, D. A., & Jonas, D. M. (2002). Solvatochromism and solvation dynamics of structurally related cyanine dyes. *J. Phys. Chem. A*, *106*, 9407–9419. doi: 10.1021/jp0205867